nature cell biology

External forces control mitotic spindle positioning

Jenny Fink[1], Nicolas Carpi[1], Timo Betz[2], Angelique Bétard[2], Meriem Chebah[1], Ammar Azioune[1], Michel Bornens[1], Cecile Sykes[2], Luc Fetler[2], Damien Cuvelier[2] and Matthieu Piel[1,3]

The response of cells to forces is essential for tissue morphogenesis and homeostasis. This response has been extensively investigated in interphase cells, but it remains unclear how forces affect dividing cells. We used a combination of micro-manipulation tools on human dividing cells to address the role of physical parameters of the micro-environment in controlling the cell division axis, a key element of tissue morphogenesis. We found that forces applied on the cell body direct spindle orientation during mitosis. We further show that external constraints induce a polarization of dynamic subcortical actin structures that correlate with spindle movements. We propose that cells divide according to cues provided by their mechanical micro-environment, aligning daughter cells with the external force field.

Proper control of the cell division axis is crucial for cell fate, development and tissue organization. In animal cells, it depends on external stimuli that polarize the cell cortex[1,2]. This polarization is transmitted to the mitotic spindle and regulates its position, which determines the axis of cell division. *In vivo*, an asymmetrical distribution of cortical cues usually results from a cell's contacts with its adhesive micro-environment—extracellular matrix and neighbouring cells[3–5]. *In vitro* cultured cells, which also exhibit regulated spindle orientation[6,7], provide the opportunity to experimentally address the contribution of physical environmental parameters, such as force, cell shape and cell–substrate adhesion, which are difficult to measure and modulate independently *in vivo*. Such parameters are relevant for the physiology and morphogenesis of individual cells[8,9] and recent studies have started to address their role in tissue morphogenesis and polarity[10,11]. However, most studies have been conducted on interphase cells, leading to a limited understanding of how mechanical constraints can translate into a specific cell response—a process called mechanotransduction[8,12]. In previous work[7,13], we placed cells on adhesive micropatterns, and showed that adhesion geometry alone can dictate the axis of cell division in cultured cells. Here, we investigated how these geometrical cues control mitotic spindle orientation. We show that adhesion geometry imposes a force field, which is signalling throughout mitosis to dynamically polarize the mitotic cell body, eventually leading to spindle orientation.

RESULTS

The distribution of retraction fibres during mitosis dictates spindle orientation

While cells round up in mitosis, they remain connected to the adhesive substrate through retraction fibres (Fig. 1a), membrane tubes filled with actin filaments[14]. These fibres have been proposed to recruit polarizing factors to the cell cortex, leading to spindle orientation[13]. However, retraction fibres may simply be historical marks of interphase cell polarity and have no role in spindle orientation. To directly address this question we carried out laser ablation of retraction fibres during late prometaphase and followed spindle orientation by visualization of the chromosome plate. Cells were plated on two different adhesive micropattern shapes to control the spatial distribution of retraction fibres[15]: a bar, generating two opposite sets of retraction fibres, and an asymmetrical cross, generating four sets of retraction fibres (Fig. 1b,c). Without laser ablation, most mitotic spindles aligned with the long axis of the respective micropattern (Supplementary Fig. S1) showing only slight rotation between late prometaphase and metaphase (10°–15°, Fig. 1d). We observed no significant spindle rotation when retraction fibres were ablated on both sides of cells dividing on bar patterns, leaving no retraction fibres on the cell periphery (16° ± 12°, Fig. 1b–d and Supplementary Fig. S2). Strong rotation of the mitotic spindle occurred only in cells dividing on cross patterns, when retraction fibres facing mitotic spindle poles were ablated (76° ± 21°, Fig. 1b–d and Supplementary Fig. S2), leading to spindle alignment with the remaining two sets of retraction fibres. Additional effects of retraction fibre ablation were a metaphase delay—probably due to destabilization of the metaphase plate (Fig. 2a, second row at 24 min)—and a significant but transient deformation of the cell body (Fig. 2a,b). Those behaviours occurred on both bar and cross patterns, excluding their impact on the strong spindle rotation observed on cross patterns. Thus, ablation experiments directly demonstrated that retraction fibres provide external cues during mitosis to orient the mitotic spindle.

Retraction fibres exert strong forces on the mitotic cell body

Cell deformation on retraction fibre ablation indicated that retraction fibres exert pulling forces on the cell body (Fig. 2a,b). Furthermore,

[1]Institut Curie, CNRS UMR 144, 26 rue d'Ulm, 75248 Paris Cedex 05, France. [2]Institut Curie, CNRS UMR 168, 26 rue d'Ulm, 75248 Paris Cedex 05, France.
[3]Correspondence should be addressed to M.P. (e-mail: matthieu.piel@curie.fr)

Received 16 July 2010; accepted 26 April 2011; published online 12 June 2011; DOI: 10.1038/ncb2269

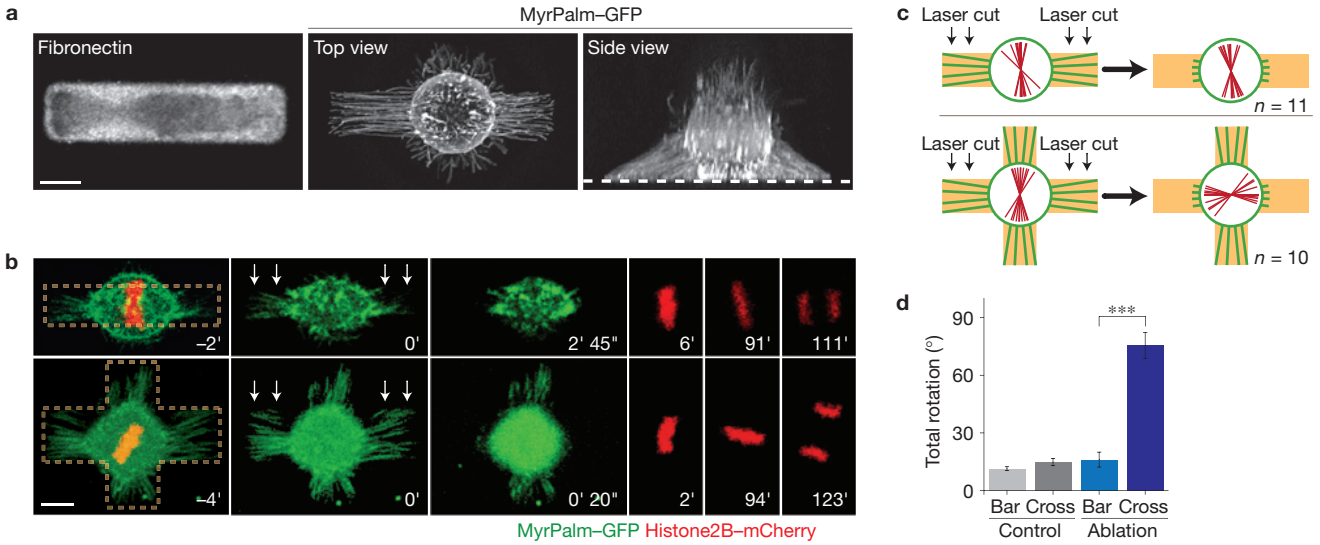

Figure 1 Retraction fibre distribution dictates mitotic spindle orientation. (**a**) HeLa cell dividing on a bar-shaped fibronectin micropattern (left) and expressing MyrPalm–GFP to visualize the plasma membrane (middle and right). A maximum intensity projection (top view of the cell, middle) and three-dimensional reconstruction (side view, right) of 85 deconvoluted *Z*-stack planes at 0.3 μm intervals are presented. (**b**) Mitotic HeLa cells on bar- (top row) or cross-shaped (bottom row) micropatterns (outlined by the orange dashed line). Cells are expressing MyrPalm–GFP (green) and histone2B–mCherry (red) to visualize plasma membrane/retraction fibres and chromosomes. Retraction fibres orthogonal to the chromosome plate were laser ablated (white arrows at 0 min). To show both cell body and retraction fibres, two *Z* planes were superposed in the green channel for the first image in the top row. Other images are single confocal slices. Time is in min (′) and s (″). (**c**) Observed chromosome plate orientation (red lines) on bar- and cross-shaped micropatterns (orange) before and after cutting. Retraction fibres/plasma membrane, green. (**d**) Total rotation (final − initial angle) of the metaphase plate in control cells and in cells after retraction fibre ablation. $n = 207$ (bar control), 69 (cross control), 11 (bar ablation) and 10 (cross ablation). Error bars represent standard error. ∗∗∗, *P* value <0.0001 (Student's *t*-test). Scale bars, 10 μm.

it has been shown that cells spread along retraction fibres during telophase[14], implying that retraction fibres can bear the forces involved in post-mitotic cell respreading[16]. Forces exerted by retraction fibres may thus be key polarizing signals during mitosis, similar to forces triggering mechanotransduction processes during interphase[8,12].

Optical tweezers measurements carried out on retraction fibres confirmed that they exerted strong pulling forces (Fig. 2c–e; see Methods for details). Fibres accessible to tension measurement had an average length of 13 ± 3 μm ($n = 20$) from the substratum to the cell body. They had a tension of 245 ± 42 pN ($n = 116$ on 20 fibres), leading to a total force of about ∼7 nN exerted on each side of a cell dividing on a bar-shaped pattern (there is an average of 27 ± 3 retraction fibres per cell side ($n = 26$ on 13 cells)). Such forces can significantly deform cells[17] and are consistent with the cell body deformation observed in metaphase cells dividing on bar-shaped patterns (6 ± 0.9%, $n = 30$, Fig. 2f and Supplementary Fig. S3). Mitotic cells attached to bar patterns were treated with drugs to inhibit actin filament assembly or myosin II motor activity. This treatment led to an elongation of the cell body in the axis of the retraction fibres. Conversely, treating cells with calyculin A, which increases myosin activity[18], resulted in significant rounding of the cell body (Fig. 2f and Supplementary Fig. S3). Mitotic cell shape thus depends on internal contractility acting against resisting forces exerted by retraction fibres (a detailed model of cell rounding has recently been proposed[19]). Retraction fibre ablation perturbed this force balance, leading to cell contraction in the axis of the ablated fibres and/or expansion in the perpendicular direction (Fig. 2g). Cells then slowly adapted to the new force field, eventually becoming round again, with a timescale similar to interphase cells adjusting their contractility to external loads[20]. On the bar pattern, no external force remained after ablation, whereas on the cross pattern cells contracted against the remaining retraction fibres perpendicular to the initial axis, which was followed by spindle rotation. We conclude that a given adhesion geometry, by imposing the distribution of retraction fibres during cell rounding, generates a specific force field on the mitotic cell body, which in turn leads to a polarized contraction of the mitotic cell: the rounding cell pulls stronger in the axis where more retraction fibres are present.

External forces exerted on mitotic cells can induce spindle rotation

To directly test the role of external forces acting through retraction fibres, we carried out a uni-axial stretch of ∼25% on mitotic cells dividing on fibronectin-coated silicon thin films (Fig. 3a and Supplementary Fig. S4a). Using ring-shaped patterns of fibronectin allowed pulling directly on retraction fibres. As the main drawback of cell stretching is its direct effect on cell shape, we used elliptical patterns designed to produce a perfectly circular ring after the stretch, avoiding the well-known effects of elongated cell shape on spindle orientation[21] (see Methods for details). During uni-axial stretching, the ends of the retraction fibres in contact with the substrate followed the deformation of the pattern, leading to an elongation of retraction fibres aligned with the stretch and a shortening of orthogonal retraction fibres (∼25% stretching of the silicon substrate in one axis induces retraction of ∼10% in the perpendicular direction). Other fibres tilted towards the direction of the stretch (Fig. 3b) without moving their contact point on the mitotic cell body. Such observations allowed us to estimate the force field resulting from the stretching process (Fig. 3c): we assumed that the ends of the retraction fibres bound to the substrate moved with the pattern deformation whereas fibre ends on the cell cortex

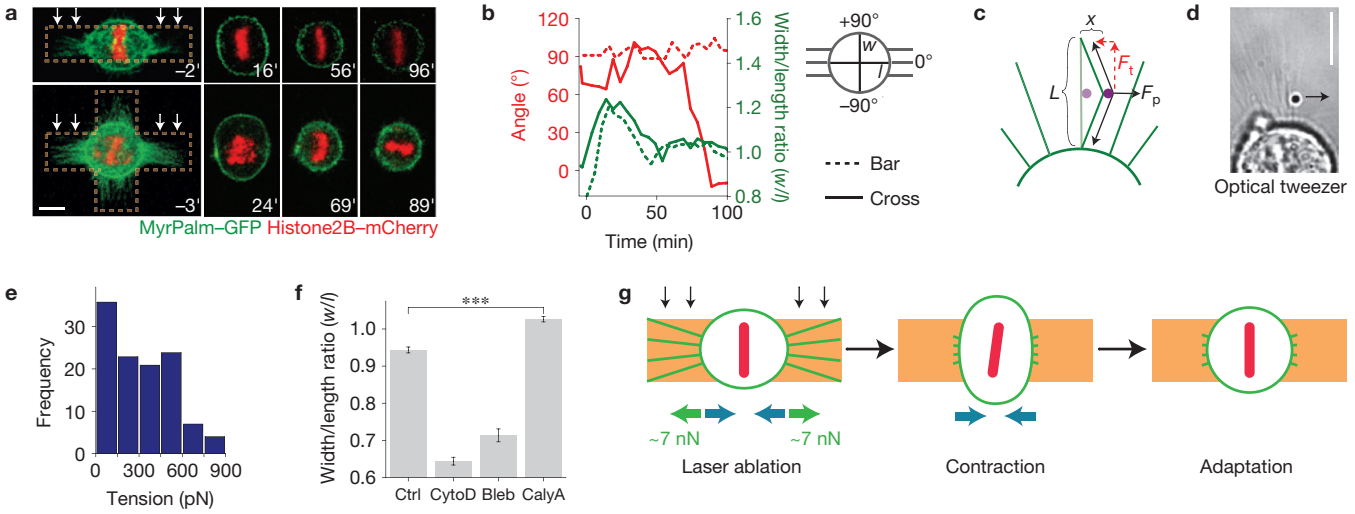

Figure 2 Retraction fibres exert strong forces on the mitotic cell body. (**a**) Mitotic HeLa cells on bar- and cross-shaped micropatterns (outlined by orange dashed lines) before and after ablation (white arrows) of retraction fibres at 0 min. Cells expressing MyrPalm–GFP (green) and histone2B–mCherry (red) to visualize membrane/retraction fibres and chromosomes. The first images show a superposition of two *Z* planes in the green channel. The other images are single confocal slices. The first row shows the same cell as in Fig. 1. Time is in min (′). (**b**) Chromosome plate angle (red) versus cell shape (width/length ratio, green) before and after retraction fibre ablation. The plots correspond to cells shown in **a** (bar, dotted line; cross, solid line). (**c**) Forces in retraction fibres measured with optical tweezers. *L*, retraction fibre length; *x*, bead displacement; F_p, pulling force of optical tweezers; F_t, tension of retraction fibre. For $x \ll L$, $F_t = F_p \times L/(4x)$. Green, membrane; violet, bead. (**d**) Phase-contrast image showing a cell body and retraction fibres with an attached bead. Optical tweezers pulling direction (arrow). (**e**) Measured tension in retraction fibres; $n = 116$ on 20 fibres. (**f**) Shape factor of drug-treated cells dividing on bar-shaped micropatterns. $n = 30$ (control, Ctrl), 54 (cytochalasin D, CytoD), 55 (blebbistatin, Bleb) and 43 (calyculin A, CalyA). Error bars represent standard error. ***, *P* value <0.0001 (Student's *t*-test). (**g**) Model for cell shape changes after laser ablation (black arrows). Intercellular contractility (blue arrows). Resisting retraction fibres (green arrows). Membrane/retraction fibres, green; chromosome plate, red; micropattern, orange. Scale bars, 10 μm.

did not move, leading to a well-defined tilt of the fibres. We assigned to each fibre a tension equal to the measured average tension and we calculated the resulting force in each axis, taking into account the contact angle of the retraction fibres with the cell body: after stretching, the main force axis was found to be parallel to the stretching direction. Mitotic spindles turned towards the stretching axis, whereas in cells dividing on un-stretched oval rings spindles aligned with the long axis of the pattern and cells plated on un-stretched circular rings exhibited a random spindle orientation (Fig. 3d–f and Supplementary Fig. S4b,c and Movie S1). Importantly, when cells were treated with low doses of the microtubule-depolymerizing drug nocodazole, perturbing astral microtubules but allowing anaphase to proceed, no rotation of the spindle was induced by stretching (Fig. 3f and Supplementary Fig. S4d). These results demonstrate that the mitotic spindle rotates to align with the forces produced by retraction fibres and that this rotation requires a normal astral microtubule array.

Mitotic cells exhibit a dynamic subcortical actin network biased by adhesion geometry

Forces exerted on mitotic *Dictyostelium discoideum* cells induce recruitment of myosin II and of the actin crosslinker cortexillin, followed by local contraction[22]. Moreover, in mitotic PtK2 cells myosin II and actin accumulate at the base of retraction fibres[14]. Forces exerted by retraction fibres may thus induce recruitment of acto-myosin structures, leading to cell polarization and spindle orientation. Labelling actin filaments in fixed mitotic cells dividing on bar patterns (Fig. 4a,b) revealed polarized subcortical actin structures facing retraction fibres. Surprisingly, these structures were often found only at one side of the cell (Fig. 4a,b). Expression of Lifeact–mCherry[23] or GFP–Utr-CH (the calponin homology domain of utrophin tagged with green fluorescent protein[24])—both binding to actin filaments without affecting their dynamics—visualized these subcortical structures and showed that they were highly dynamic in HeLa and RPE1 cells (Fig. 4c and Supplementary Figs S5, S6 and Movies S2–S6). Similar dynamic actin structures have recently been observed in various cell types and have been shown to specifically appear in mitosis[25]. Their apparent movement is the result of fast polymerization/depolymerization cycles[25]. We observed that cells dividing on disc patterns, which exhibit a homogeneous distribution of retraction fibres, showed circulating actin subcortical structures throughout mitosis, as reported previously[25] (Fig. 4c and Supplementary Movie S2). On patterns imposing an inhomogeneous distribution of retraction fibres, such as cross or bar patterns, actin structures were also dynamic, but appeared more intense when facing retraction fibres (Fig. 4c and Supplementary Movies S3 and S4). To quantify this polarization process, we analysed kymographs of time-lapse images of actin structures, taken in the main axis of the pattern (or in the axis of the mitotic spindle for the disc), and in the orthogonal axis (Fig. 5a). We measured the time actin structures spent in each sector of the cell (marked S1–S4 in Fig. 5a, quantified in Fig. 5b and Supplementary Table S1), their total intensity in each sector integrated in space and time (Fig. 5c and Supplementary Table S1) and the depth at which they penetrate into the cytoplasm (Fig. 5d and Supplementary Table S1). These data showed that subcortical actin structures rotated below the cell cortex approximately at the same speed (60°–70° min^{-1}, Supplementary Table S1) for all examined pattern shapes. For cells dividing on disc patterns, structures were as strong and went as deep inside the cell at 90° of the spindle axis as they did in the axis of the spindle, thus showing no bias. However, in

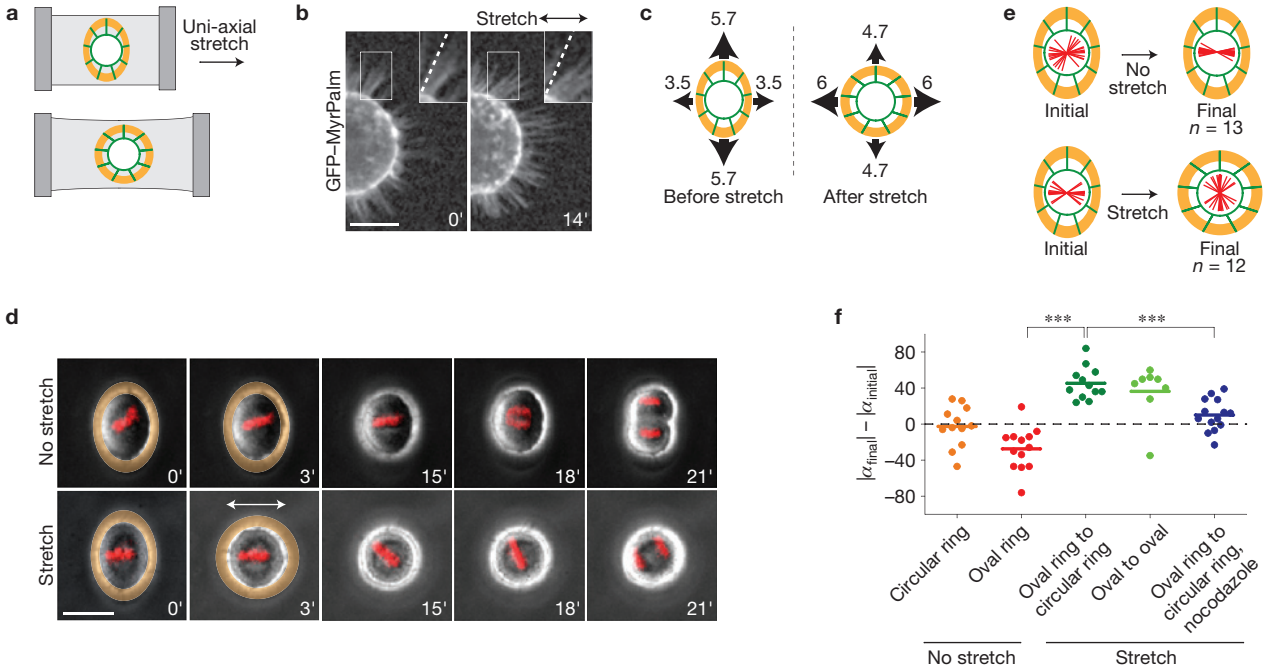

Figure 3 Stretching retraction fibres induces spindle rotation. (**a**) Cell stretching set-up. Membrane, green; micropattern, orange. (**b**) Mitotic HeLa cell expressing MyrPalm–GFP to visualize membranes. Maximum intensity projections of deconvoluted *Z* stacks. The insets show a 1.5-fold magnification. The dashed lines represent the orientation of the retraction fibre before stretching. (**c**) Calculated force field before and after stretching. Black arrows and numbers represent total forces (nN) in *X* and *Y* axes. (**d**) RPE1 cells dividing on silicon substrates with oval ring micropatterns (orange). The pictures are a superposition of phase-contrast images and the Hoechst 33342 signal (red) to visualize the DNA/chromosomes. Horizontal stretch (white arrow) just after image acquisition at 0 min. (**e**) Chromosome plate orientation (red lines) in controls (upper row) and stretched cells (lower row). The initial orientation shows the orientation in the first recorded image and the final orientation shows the orientation at anaphase onset. Membrane, green; pattern, orange. (**f**) Scatter plot showing net rotations (α) of chromosome plates for controls and stretched cells. Negative values represent rotation towards 0° (final angle for controls on oval ring patterns); positive values represent rotation towards 90°. $n = 12$ (circular ring), 13 (oval ring), 12 (oval ring to circular ring), 8 (oval to oval) and 14 (oval ring to circular ring, nocodazole). ***, *P* value <0.0001 (Student's *t*-test). Time is in min (′). Scale bars, 10 μm (**b**) and 20 μm (**d**).

the case of the bar and the asymmetric cross, they were both more intense and went deeper inside the cell in the main axis of the pattern than in the orthogonal axis. Results on disc patterns proved that the spindle alone did not induce the polarization of the subcortical actin structures. Furthermore, when cells were treated with low doses of nocodazole leading to loss of spindle alignment with the bar pattern, actin polarization remained in the axis of the retraction fibres and did not follow the spindle poles (Fig. 6). Together our results show that the intensity and penetration depth of subcortical actin structures into the cytoplasm depend on the distribution of retraction fibres.

Retraction fibres dynamically control subcortical actin polarization in mitotic cells

The impact of retraction fibres on subcortical actin can be directly tested by laser ablation on cross shapes, as shown in Fig. 1. Indeed, after ablation of retraction fibres facing the spindle poles, actin structures repolarized along the axis of the remaining retraction fibres in 84% of cells dividing on cross patterns ($n = 19$, Fig. 7a–c and Supplementary Movie S7). This was always preceded by a short period during which actin structures appeared homogeneous along the cell periphery (~11 min, Fig. 7d). When all retraction fibres were ablated (bar pattern), actin structures either lost their polarization bias towards the long axis of the bar and did not repolarize in the orthogonal axis (7/16 cells, Fig. 7a,b and Supplementary Movie S8) or kept a bias in the original axis (7/16 cells). We followed in parallel the mitotic spindle, labelled by microtubule plus-end binding protein 3 (EB3)–GFP. The spindle rotated by more than 40° in 81% of cells that showed repolarization after ablation on cross patterns (average rotation 56° ± 7, Fig. 7e), but only in 6% of cells after ablation on bar patterns (average rotation 15° ± 3). Importantly, spindle rotation always followed actin repolarization with an average delay of ~5 min (Fig. 7d), indicating that actin structure repolarization may be responsible for spindle rotation.

Subcortical actin structures exert pulling forces on the mitotic spindle

In many systems, spindle positioning depends both on actin and microtubules[1]. Interestingly, more than 20 years ago it was observed that centring forces acting on microtubule asters in sand dollar eggs were generated in the cytoplasm and not at the cell cortex[26]. This observation has recently been confirmed in other systems for mitotic spindle positioning[27,28]. It is thus tempting to speculate that motors bound to subcortical or cytoplasmic actin structures may be responsible for generating these cytoplasmic forces acting on astral microtubules in mitosis. Dynamic subcortical/cytoplasmic actin structures have previously been described in mice meiotic oocytes[29,30] and in mitotic cells in *Xenopus* embryos[31] and they have been proposed to play a role in spindle positioning and elongation, even if not necessarily acting through astral microtubules. Here we show that in somatic mammalian cells, such actin structures also

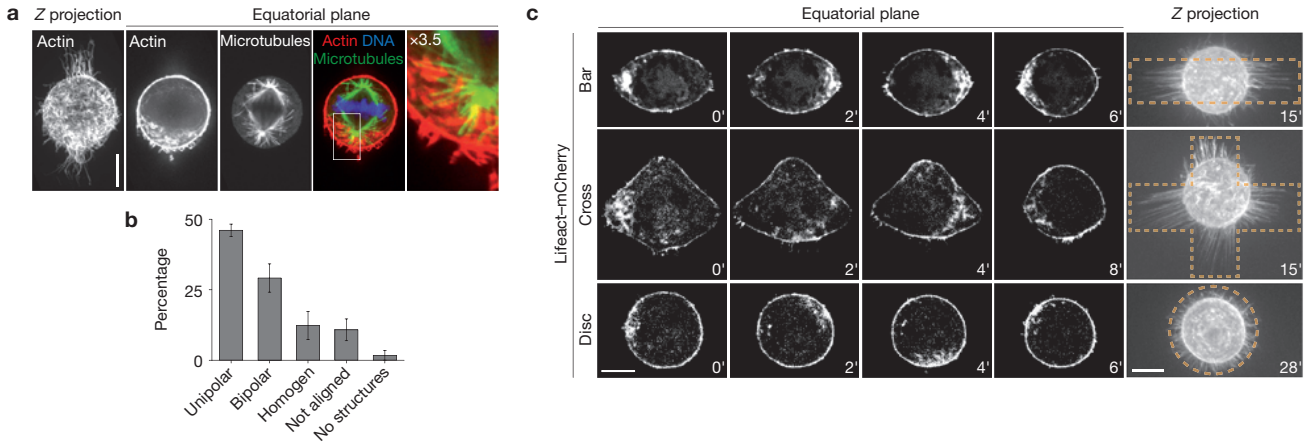

Figure 4 Adhesion geometry can bias dynamic subcortical actin structures in mitotic cells. (**a**) HeLa cells dividing on 12 μm fibronectin lines were fixed, stained for actin (phalloidin), microtubules and DNA and imaged using a spinning-disc confocal microscope. (**b**) Graph representing the distribution of subcortical actin structures in fixed HeLa cells dividing on 12 μm lines ($n = 70$ from two independent experiments). 'Not aligned' means unipolar structure, but not aligned with the retraction fibre axis. Error bars represent standard error. (**c**) Mitotic HeLa cells on bar- (first row), cross- (second row) and disc-shaped (third row) micropatterns (dashed orange lines). Cells are stably expressing Lifeact–mCherry to visualize filamentous actin. The equatorial plane of cells was imaged during mitotic cell rounding. Images for *Z* projections, on the right, were acquired at 1 μm intervals, after complete cell rounding. Images for cells dividing on bar and disc shapes were mirrored to align with the cell on the cross shape. Scale bars, 10 μm. Time is in min (′).

exist and that they are oriented by the adhesive geometry of the micro-environment, probably due to external forces acting on the cell body. When polarized, such structures may induce spindle movement and alignment. As a consequence, the mitotic spindle should move towards newly formed actin structures, leading to oscillations in phase with oscillating actin structures for cells dividing on bar patterns. We thus looked closely at time-lapse movies of cells expressing both an actin marker (Lifeact–mCherry) and a microtubule marker (EB3–GFP). As expected the mitotic spindle often moved towards subcortical actin structures (Fig. 8a). To quantify this behaviour, we analysed kymographs of both Lifeact–mCherry and EB3–GFP signals (see Methods, Fig. 8b–e). We calculated, for each occurrence of a clearly polarized actin structure, whether the net movement of the spindle was towards or away from the structures. We found that spindles moved towards actin structures in 66% and away from them in only 23% of all cases (Fig. 8f,g). When astral microtubules were specifically depolymerized with low doses of nocodazole, leading to misalignment of the spindle with the bar pattern, this correlation was lost (Fig. 8f,g). These results indicate that subcortical actin structures, or associated protein complexes, probably provide pulling forces aligning the mitotic spindle with the pattern axis.

Cytoplasmic actin structures assembled and disassembled on very short timescales, rotating at a speed of about 70° min^{-1} in cells plated on disc patterns (or about 12 μm min^{-1} along the cell periphery), whereas the maximum speed recorded for the spindle was about 8° min^{-1} (not shown). Cytoplasmic actin structures thus moved at a much higher speed than the mitotic spindle. When actin structures exhibit no bias as they travel around the cell, short-timescale microtubule/actin interactions would lead to a null average force on the spindle, explaining the reduced spindle rotation on disc patterns[7]. On the other hand, when actin structures are more dense, and penetrate further inside the cell at given locations, as observed at cell sides facing retraction fibres on the bar pattern, interaction with astral microtubules would be more likely in these directions, resulting in a net force aligning the spindle.

DISCUSSION

Here, we provide direct experimental proof that external forces can induce mitotic spindle rotation in human cells. We propose that these forces bias dynamic subcortical actin structures that interact with astral microtubules, leading to mitotic spindle alignment with the external force field. The effects of external forces on polarization of actin structures have been extensively studied in interphase cells[12,32], and similar mechanisms may also be active during mitosis to orient the mitotic spindle. Indeed, Src tyrosine kinases, known mechanosensors[8], have been shown to control mitotic spindle orientation[7], although the exact mechanism remains to be elucidated. Our results open directions for future research. Cytoplasmic actin structures acting on the meiotic/mitotic spindle have been identified in mice oocytes and in *Xenopus* embryos[29,30]. Our work, in agreement with a previous study[25], indicates that these structures may be universal and not restricted to early stages of development. These structures, which have been shown to depend on formins in mice oocytes, are dependent on actin-related protein 2/3 (Arp2/3) in somatic cells (our unpublished results and ref. 25). It is possible that both types of structure exist at different degrees in different cell types, with distinct functions in mitosis, similarly to what is known for interphase cells. These Arp2/3-dependent structures were often more intense during the rounding process (data not shown), indicating that they depend on forces exerted on cells.

Further experiments will be required to unravel the molecular links between these structures and astral microtubules. Interestingly, in HeLa cells it has been observed that whereas G protein α_{i1} ($G\alpha_{i1}$) seems strictly cortical, $G\alpha_{i2}$ also exhibits a strong cytoplasmic staining. In Fig. 3a of ref. 33, this staining appears polarized, strongly resembling cytoplasmic actin structures that we have described. This is indicative of an interesting dual cortical and cytoplasmic recruitment of the classical $G\alpha_i$–LGN (G-protein signalling modulator 2)–NuMa (microtubule-binding nuclear mitotic apparatus protein) pathway on specific cortical and subcortical actin structures, the second depending on external forces acting on the mitotic cell. The dynamic

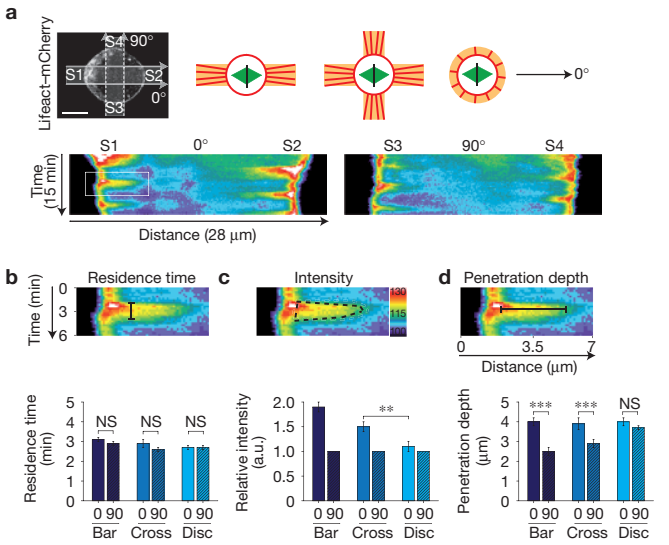

Figure 5 Quantification of subcortical actin polarization for different adhesion geometries. (**a**) Kymographs of 70 pixels in width were created from time-lapse movies (15 s) of cells expressing Lifeact–mCherry (top left picture). Cells were dividing on bar-, cross- and disc-shaped patterns (scheme: fibronectin pattern, orange; actin (retraction fibres, cortex), red; spindle, green; chromosome plate, black). Kymographs were generated in the main axis of the retraction fibres (bar and cross shape; 0°) or in the axis of the mitotic spindle (disc shape; 0°) and orthogonal to it (90°) as indicated by the arrows (top left picture). The second row shows a representative example of the resulting kymographs for a cell dividing on a bar-shaped pattern. (**b**–**d**) Residence time (**b**), total intensity (**c**) and penetration depth (**d**) of actin structures measured using kymographs generated along 0° and 90°. The first row shows a twofold magnification of the white frame in **a**. Black lines symbolize the measured height (residence time), area (intensity) and width (penetration depth) of the Lifeact–mCherry signal. Graphs represent values for cells dividing on bar-($n = 14$), cross-($n = 13$) and disc-($n = 12$) shaped patterns in 0° and 90° axes. Error bars represent standard error. NS, not significant. **, $P = 0.018$ in **c**; ***, $P < 0.0001$ (bar) and $P = 0.01$ (cross) in **d** (Student's t-test).

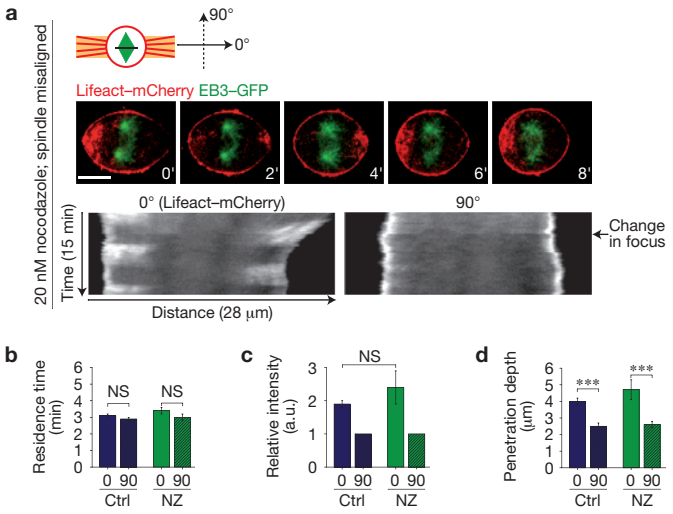

Figure 6 Polarization of dynamic subcortical actin structures persists when astral microtubules are depolymerized and the spindle is misoriented. (**a**) HeLa cell stably expressing Lifeact–mCherrry and EB3–GFP to visualize filamentous actin and spindle poles, respectively. The cell is dividing on a bar-shaped pattern as shown in the scheme (top, fibronectin pattern, orange; actin (retraction fibres, cortex), red; spindle, green; chromosome plate, black). As a result of treatment with low doses of nocodazole (20 nM), the spindle is misaligned during mitosis (middle). Kymographs were generated in the Lifeact–mCherry channel along the retraction fibre axis (0°) of the bar pattern and orthogonal to it (90°). Although the spindle poles are aligned with the 90° axis, polarization of subcortical actin structures remains in the axis of the retraction fibres (0°, bottom). (**b**–**d**) Graphs representing residence time (**b**), total intensity (**c**) and penetration depth (**d**) of actin structures along 0° and 90° axes in HeLa cells dividing on a bar-shaped pattern (see Fig. 5 for measurement). Cells were treated with either dimethylsulphoxide (Ctrl, 0.2%, $n = 14$) or nocodazole (NZ, 20 nM, $n = 15$). Error bars represent standard error. NS, not significant. ***, $P < 0.0001$ for 'Ctrl' and $P = 0.0060$ for 'NZ' (Student's t-test). Scale bar, 10 μm. Time is in min (').

nature of these structures also remains to be understood. Dynamic structures rather than static ones may improve spindle centring: if actin structures recruit microtubule anchoring and stabilizing factors, a static polarized actin meshwork is likely to move the spindle off centre, which may induce asymmetric cell division. It is also possible that spindle rotation is more efficient when astral microtubules from both spindle poles are alternatively being pulled on, whereas a single static polarized structure would move the spindle rather than rotate it efficiently. A full understanding of the interaction of dynamic astral microtubules with dynamic actin structures bearing pulling forces will require both mathematical modelling and further more-direct experiments.

It is well known that growth and movements in tissues generate local constraints on cells[10,11]. Our results indicate that these constraints may guide the cell division axis and thus be important for morphogenesis. In plants, constraints generated by growing cells have been shown to influence the cell growth axis, such a feedback being enough to explain a large part of the morphogenetic process[34]. In growing animal tissues, cells in certain regions (most likely peripheral regions) may be subjected to extension forces, whereas others (most likely central regions) may be under compression. Aligning the cell division axis with the local force field may release the stress stored during the growth process in regions in which cells are in extension. This would fluidize the tissues, allowing it to undergo extensive deformation while growing[35]. Such a process is predicted to be especially important for fast-growing tissues with short cell division times, undergoing large deformations, typical of early development of vertebrate embryos, for which internal constraints due to growth cannot be compensated by cell–cell rearrangements. We propose that cells have evolved to use all possible sources of information, including mechanical signals, leading to a more robust determination of their division axis. □

METHODS

Methods and any associated references are available in the online version of the paper at http://www.nature.com/naturecellbiology

Note: Supplementary Information is available on the Nature Cell Biology website

ACKNOWLEDGEMENTS

We are grateful to J. Colombelli for helpful discussions and preliminary experiments on retraction fibre cutting; L. Mahadevan for helpful discussions concerning mechanical cortex anisotropy; D. Gerlich (ETH, Zurich, Switzerland) and R. Tsien (UCSD, San Diego, USA) for the pIRES-puro3–MyrPalm–GFP plasmid; V. Doye (IJM, Paris, France) for the pIRES-neo–histone2B–mCherry plasmid; W. Bement (University of Wisconsin, Madison, USA) for the GFP–Utr-CH plasmid; R. Wedlich-Soldner (IMPRS, Martinsried, Germany) and G. Montagnac (Institut Curie, Paris, France) for the Lifeact–mCherry plasmid; M. Heuze (Institut Curie, Paris, France) and A. M. Lennon-Dumesnil (Institut Curie, Paris, France) for the Lifeact–mCherry lentivirus; V. Fraisier, the Nikon Imaging Center and the PICT–IBiSA of the

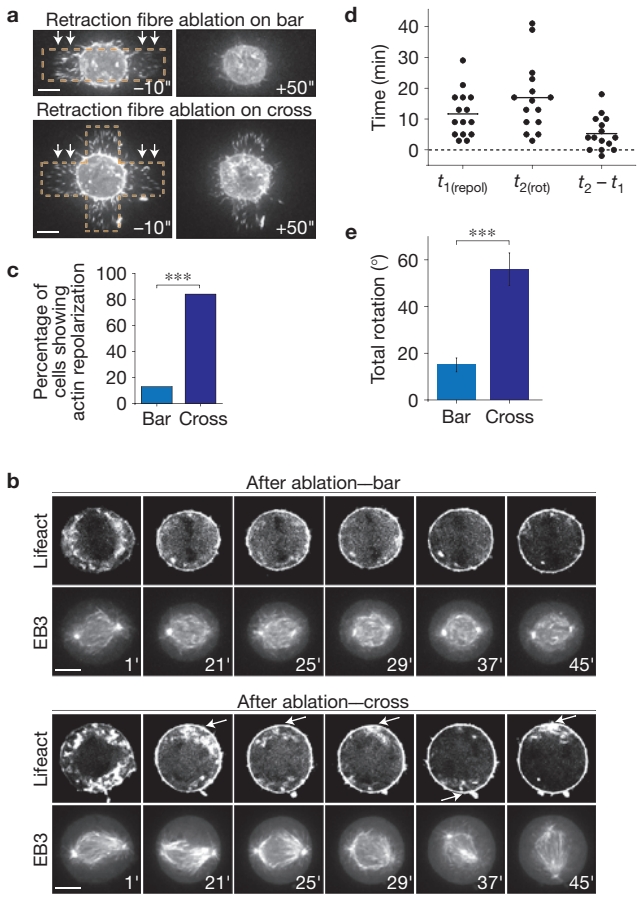

Figure 7 Mitotic spindle rotation and movement strongly correlate with polarization of dynamic subcortical actin structures. (**a**) Ablation of retraction fibres (white arrows) in cells dividing on bar (top panel) and cross patterns (bottom panel). Retraction fibres are visualized by Lifeact–mCherry expression and are cut at 0 s. Patterns, dashed orange lines. (**b**) Evolution of subcortical actin structures (Lifeact–mCherry) and the mitotic spindle (EB3–GFP) after retraction fibre ablation of the cells shown in **a**. Cell dividing on a bar pattern (top panel); cell dividing on a cross pattern (bottom panel). White arrows highlight regions with a higher density of subcortical actin structures. (**c**) Quantification of actin structure behaviour after ablation of retraction fibres. Actin repolarization means polarization of subcortical structures in the axis orthogonal to the ablated retraction fibres. Repolarization was taken into account only when lasting longer than 10 consecutive minutes. $n = 16$ for bar shape; $n = 19$ for cross shape. ***, $P = 2 \times 10^{-5}$ (Chi-square test). (**d**) Graph representing the time when actin starts to repolarize in the axis orthogonal to retraction fibre cutting ($t_{1(repol)}$), time when the spindle starts to rotate ($t_{2(rot)}$) and the delay between the start of actin repolarization and the start of spindle turning (t_2–t_1). Ablation is at $t = 0$. (**e**) Quantification of spindle behaviour after ablation of retraction fibres. Total rotation means maximum spindle rotation towards the axis orthogonal to retraction fibre cutting. $n = 16$ for bar shape; $n = 19$ for cross shape. Error bars represent standard error. ***, $P < 0.0001$ (Student's t-test). Scale bars, 10 μm. Time is in s (″, **a**) and min (′, **b**).

Institut Curie for technical support in microscopy; J. Boulanger for image treatment using ndsafir; and Z. Maciarowski, C. Guérin and A. Viguier for FACS sorting of stable cell lines. We thank M. Thery and J. Aubertin for helpful discussions throughout the course of this work and A. W. Murray, E. Paluch, A. M. Lennon-Dumesnil, A. Taddei, M. Thery, S. Misery-Lenkei and members of the Piel laboratory for critical reading of the manuscript. This work was supported by the Centre National de la Recherche Scientifique, the Institut Curie and by ANR (ANR-06-PCVI-0010) and HFSP grants to M.P. J.F. was supported by pre-doctoral fellowships from Boehringer Ingelheim Fonds and the Association pour la Recherche sur le Cancer.

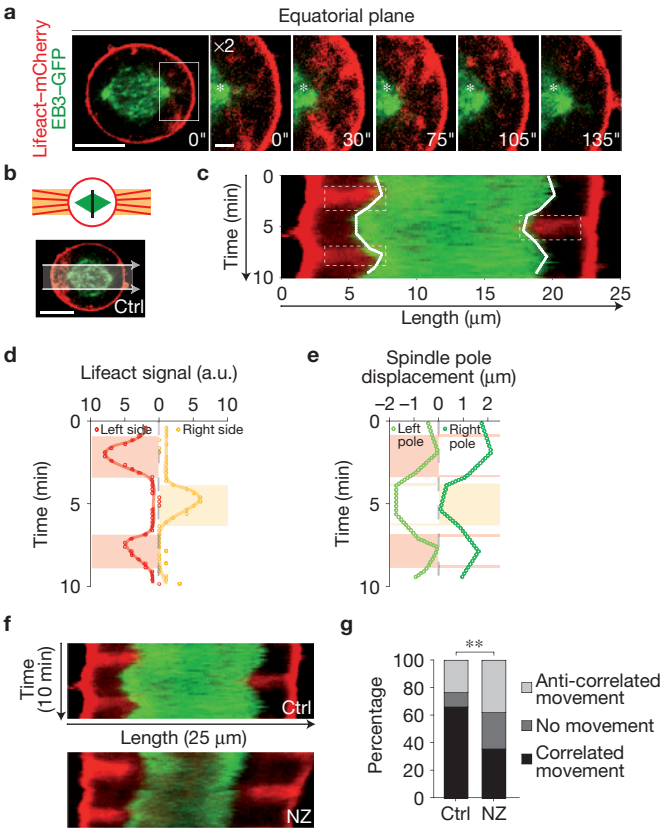

Figure 8 Subcortical actin structures exert pulling forces on the mitotic spindle. (**a**) Time-lapse sequence of a HeLa cell stably expressing Lifeact–mCherry and EB3–GFP. The white asterisk marks the position of the spindle pole at time zero. Scale bars, 10 μm (first image) and 2 μm (second image). Time is in s (″). (**b**) A HeLa cell dividing on a bar pattern (as shown in the scheme: fibronectin pattern, orange; actin (retraction fibres, cortex), red; spindle, green; chromosome plate, black) and stably expressing Lifeact–mCherry and EB3–GFP to visualize actin filaments and spindle poles. Equatorial planes were imaged every 15 s using a spinning-disc confocal microscope. Kymographs of 70 pixel in width were created parallel to the spindle as indicated by the white bar and arrows in the picture. Scale bar, 10 μm. (**c**) Kymograph resulting from **b**. The dashed white areas highlight the actin signal; the white lines highlight spindle boundaries. (**d**) Lifeact–mCherry temporal profile corresponding to the kymograph shown in **c** (red signal) for the right and the left side of the cell. (**e**) Spindle pole displacement corresponding to the kymograph shown in **c** as determined by automated detection of the spindle boundary in the kymograph (green signal). Note that the spindle always changes direction with a delay, to eventually move towards the structures. (**f**) A HeLa cell dividing on a bar-shaped pattern as shown in **b**. Kymographs were generated along the retraction fibre axis in the Lifeact–mCherry and EB3–GFP channel according to **b**. Resulting kymographs of control cells (Ctrl, first row) and nocodazole-treated (NZ, 20 nM, second row) cells. Note that the spindle does not oscillate anymore in NZ-treated cells. (**g**) Quantification of spindle pole movements with respect to subcortical actin structures of control- (Ctrl, $n = 47$ for 12 cells) and nocodazole- (NZ, 20 nM; $n = 42$ for 11 cells) treated cells; correlated movement means spindle movement towards actin structures; anti-correlated means movement away from actin structures. **, P value is 0.014 (Chi-square test).

AUTHOR CONTRIBUTIONS

J.F. designed, carried out and analysed most experiments and wrote the article, N.C. carried out most cell stretching experiments as well as experiments shown in Fig. 2f and Supplementary Fig. S3, T.B. carried out and analysed optical trap experiments (Fig. 2c–e), A.B. carried out some cell stretching experiments, M.C. carried out the experiments shown in Fig. 2f and Supplementary Fig. S3, A.A. developed the method to produce micropatterns on stretchable substrates, M.B. contributed ideas,

discussion and supervised part of the work of J.F., C.S. contributed ideas and discussion and supervised the work on optical trap experiments, L.F. carried out laser ablation experiments (Fig. 1), D.C. set up the cell stretching device, supervised the work of A.B. and contributed ideas and discussion, and M.P. supervised the work, carried out experiments and wrote the paper.

COMPETING FINANCIAL INTERESTS

The authors declare no competing financial interests.

Published online at http://www.nature.com/naturecellbiology
Reprints and permissions information is available online at http://www.nature.com/reprints

1. Gönczy, P. Mechanisms of asymmetric cell division: flies and worms pave the way. *Nat. Rev. Mol. Cell Biol.* **9,** 355–366 (2008).
2. Ahringer, J. Control of cell polarity and mitotic spindle positioning in animal cells. *Curr. Opin. Cell Biol.* **15,** 73–81 (2003).
3. Lechler, T. & Fuchs, E. Asymmetric cell divisions promote stratification and differentiation of mammalian skin. *Nature* **437,** 275–280 (2005).
4. Lu, B., Roegiers, F., Jan, L. Y. & Jan, Y. N. Adherens junctions inhibit asymmetric division in the *Drosophila* epithelium. *Nature* **409,** 522–525 (2001).
5. Fernandez-Minan, A., Martin-Bermudo, M. D. & Gonzalez-Reyes, A. Integrin signaling regulates spindle orientation in *Drosophila* to preserve the follicular-epithelium monolayer. *Curr. Biol.* **17,** 683–688 (2007).
6. Toyoshima, F. & Nishida, E. Integrin-mediated adhesion orients the spindle parallel to the substratum in an EB1- and myosin X-dependent manner. *EMBO J.* **26,** 1487–1498 (2007).
7. Thery, M. *et al.* The extracellular matrix guides the orientation of the cell division axis. *Nat. Cell Biol.* **7,** 947–953 (2005).
8. Vogel, V. & Sheetz, M. Local force and geometry sensing regulate cell functions. *Nat. Rev. Mol. Cell Biol.* **7,** 265–275 (2006).
9. Terenna, C. R. *et al.* Physical mechanisms redirecting cell polarity and cell shape in fission yeast. *Curr. Biol.* **18,** 1748–1753 (2008).
10. Farhadifar, R., Roper, J. C., Aigouy, B., Eaton, S. & Julicher, F. The influence of cell mechanics, cell–cell interactions, and proliferation on epithelial packing. *Curr. Biol.* **17,** 2095–2104 (2007).
11. Rauzi, M., Verant, P., Lecuit, T. & Lenne, P. F. Nature and anisotropy of cortical forces orienting *Drosophila* tissue morphogenesis. *Nat. Cell Biol.* **10,** 1401–1410 (2008).
12. Wozniak, M. A. & Chen, C. S. Mechanotransduction in development: a growing role for contractility. *Nat. Rev. Mol. Cell Biol.* **10,** 34–43 (2009).
13. Thery, M., Jimenez-Dalmaroni, A., Racine, V., Bornens, M. & Julicher, F. Experimental and theoretical study of mitotic spindle orientation. *Nature* **447,** 493–496 (2007).
14. Cramer, L. P. & Mitchison, T. J. Myosin is involved in postmitotic cell spreading. *J. Cell Biol.* **131,** 179–189 (1995).
15. Azioune, A., Storch, M., Bornens, M., Thery, M. & Piel, M. Simple and rapid process for single cell micro-patterning. *Lab. on a chip* **9,** 1640–1642 (2009).
16. Burton, K. & Taylor, D. L. Traction forces of cytokinesis measured with optically modified elastic substrata. *Nature* **385,** 450–454 (1997).
17. Guck, J. *et al.* The optical stretcher: a novel laser tool to micromanipulate cells. *Biophys. J.* **81,** 767–784 (2001).
18. Chartier, L. *et al.* Calyculin-A increases the level of protein phosphorylation and changes the shape of 3T3 fibroblasts. *Cell Motil. Cytoskeleton* **18,** 26–40 (1991).
19. Stewart, M. P. *et al.* Hydrostatic pressure and the actomyosin cortex drive mitotic cell rounding. *Nature* **469,** 226–230 (2011).
20. Jungbauer, S., Gao, H., Spatz, J. P. & Kemkemer, R. Two characteristic regimes in frequency-dependent dynamic reorientation of fibroblasts on cyclically stretched substrates. *Biophys. J.* **95,** 3470–3478 (2008).
21. O'Connell, C. B. & Wang, Y. L. Mammalian spindle orientation and position respond to changes in cell shape in a dynein-dependent fashion. *Mol. Biol. Cell* **11,** 1765–1774 (2000).
22. Effler, J. C. *et al.* Mitosis-specific mechanosensing and contractile-protein redistribution control cell shape. *Curr. Biol.* **16,** 1962–1967 (2006).
23. Riedl, J. *et al.* Lifeact: a versatile marker to visualize F-actin. *Nat. Methods* **5,** 605–607 (2008).
24. Burkel, B. M., von Dassow, G. & Bement, W. M. Versatile fluorescent probes for actin filaments based on the actin-binding domain of utrophin. *Cell Motil. Cytoskeleton* **64,** 822–832 (2007).
25. Mitsushima, M. *et al.* Revolving movement of a dynamic cluster of actin filaments during mitosis. *J. Cell Biol.* **191,** 453–462 (2010).
26. Hamaguchi, M. S. & Hiramoto, Y. Analysis of the role of astral rays in pronuclear migration in sand dollar eggs by the colcemid-UV method. *Dev. Growth Differ.* **28,** 143–156 (1986).
27. Minc, N., Burgess, D. & Chang, F. Influence of cell geometry on division-plane positioning. *Cell* **144,** 414–426 (2011).
28. Wuhr, M., Tan, E. S., Parker, S. K., Detrich, H. W. 3rd & Mitchison, T. J. A model for cleavage plane determination in early amphibian and fish embryos. *Curr. Biol.* **20,** 2040–2045 (2010).
29. Azoury, J. *et al.* Spindle positioning in mouse oocytes relies on a dynamic meshwork of actin filaments. *Curr. Biol.* **18,** 1514–1519 (2008).
30. Schuh, M. & Ellenberg, J. A new model for asymmetric spindle positioning in mouse oocytes. *Curr. Biol.* **18,** 1986–1992 (2008).
31. Woolner, S., O'Brien, L. L., Wiese, C. & Bement, W. M. Myosin-10 and actin filaments are essential for mitotic spindle function. *J. Cell Biol.* **182,** 77–88 (2008).
32. Yoshigi, M., Hoffman, L. M., Jensen, C. C., Yost, H. J. & Beckerle, M. C. Mechanical force mobilizes zyxin from focal adhesions to actin filaments and regulates cytoskeletal reinforcement. *J. Cell Biol.* **171,** 209–215 (2005).
33. Woodard, G. E. *et al.* Ric-8A and Gi alpha recruit LGN, NuMA, and dynein to the cell cortex to help orient the mitotic spindle. *Mol. Cell Biol.* **30,** 3519–3530 (2010).
34. Hamant, O. *et al.* Developmental patterning by mechanical signals in *Arabidopsis*. *Science* **322,** 1650–1655 (2008).
35. Ranft, J. *et al.* Fluidization of tissues by cell division and apoptosis. *Proc. Natl Acad. Sci. USA* **107,** 20863–20868 (2010).

METHODS

Cell culture, plasmid transfections and DNA labelling. HeLa cells were cultured in DMEM/Glutamax (Gibco) with 10% fetal calf serum (FCS) and antibiotics (penicillin/streptomycin; Gibco). hTERT-RPE1 cells were cultured in DMEM-F12 (Gibco) with 10% FCS, 2 mM glutamine and antibiotics (penicillin/streptomycin). Laser ablation experiments, requiring stable expression of fluorescent markers, were carried out in HeLa cells. Stretching experiments were carried out in both HeLa (Fig. 3b) and RPE1 cells (Fig. 3d–f and Supplementary Fig. S4). HeLa and RPE1 cells were cultured in Leibovitz's CO_2-independent medium without phenol red during live-cell imaging and micro-manipulation experiments.

Plasmid transfection was carried out using Lipofectamine LTX and Plus reagent (Invitrogen). pBOS-histone2B–mCherry–IRES–neo, pIRES-puro–MyrPalm–GFP, pIRES-puro–Lifeact–mCherry and pEGFP-N3–EB3 plasmids were used. Positive cells were selected with G418 (0.5 mg ml^{-1}) or puromycin (0.33 μg ml^{-1}) and subsequent fluorescence-activated cell sorting (FACS). The pCS2–GFP–Utr-CH vector was transiently transfected.

To generate a stable RPE1 cell line, we infected RPE1 cells with a vesicular stomatitis virus G (VSVG)-pseudotyped human immunodeficiency virus (HIV)-derived lentivirus containing the Lifeact–mCherry DNA. Positive cells were selected for medium expression of Lifeact–mCherry using FACS sorting.

DNA in living RPE1 cells was stained with 0.1 μg ml^{-1} Hoechst 33342 for 15 min.

Cell fixation and staining. All solutions were made using BRB80 buffer. Cells were pre-extracted and fixed for 1 min using 4% paraformaldehyde, 0.25% glutaraldehyde and 0.05% NP-40, then fixed for 10 min in 4% paraformaldehyde and 0.25% glutaraldehyde and finally treated with 0.1 M NH_4Cl for 10 min. Actin and DNA were stained using AlexaFluor594-phalloidin (Invitrogen) and DAPI (4,6-diamidino-2-phenylindole). Microtubules were immunolabelled using anti-α-tubulin (1:2,000, mouse, clone B-5-1-2, Sigma) and secondary anti-mouse-Alexa488 antibody (Jackson ImmunoResearch Laboratories).

Drug treatments. Cells were incubated with 50 μM blebbistatin, 1 μg ml^{-1} cytochalasin D and 20 nM nocodazole, for 30 min, or 10 nM calyculin A for 15 min before fixation.

For specific depolymerization of astral microtubules, HeLa and RPE1 cells were incubated with 20 nM nocodazole for 1 h before image acquisition. This concentration, although severely affecting astral microtubules (Supplementary Fig. S4d), did not prevent RPE1 cells from entering anaphase with normal timing.

Micropatterning on glass and flexible substrates. Adhesive fibronectin micropatterns were produced using deep-ultraviolet illumination through a photomask as previously described[15]. To bind PLL-g-PEG (poly(L-lysine)-grafted-poly(ethylene glycol)), silicon membranes were illuminated for 5 min using deep ultraviolet and incubated with a solution of *N*-hydroxysuccinimide (160 mM) and *N*-(3-dimethylaminopropyl)-*N*′-ethyl-carbodiimide-hydrochloride (350 mM) for 30 min. After quick rinsing, PLL-g-PEG (1 mg ml^{-1} in 10 mM HEPES, pH 8.5) was incubated for 1 h (ref. 36).

Ablation experiments. Ablation experiments (Figs 1, 2 and Supplementary Fig. S2) were carried out on mitotic cells during late prometaphase, as soon as a clear chromosome plate could be detected. The two-photon laser scanning microscope set-up used was an LSM510 Meta (Zeiss) equipped with a ×40 0.8 water immersion objective and coupled to a Maitai DeepSee femtosecond laser (690–1,020 nm; Spectra-Physics) and a 633 nm HeNe laser. Ablation was carried out in the cell adhesion plane. Noise was removed from the acquired pictures using the despeckle function of ImageJ.

For ablation in cells co-expressing Lifeact–mCherry and EB3–GFP (Fig. 7 and Supplementary Movies S7, S8), we used a Yokagawa CSU-X1 spinning head mounted on an Eclipse Ti inverted microscope (Nikon), coupled to an EMCCD (electron-multiplying charge-coupled device) 512 × 512camera (Evolve; Photometrics), and a ×1000.5–1.3 Oil Iris objective (S Fluor, Nikon). Ablation was carried out 2–3 μm above the cell adhesion plane using an iLas system interfaced with a pulsed 355 nm ultraviolet laser (Roper Scientific). The pulse was 400 ps at 10 mW, 1 μJ per pulse, scanning at 25 μs per pixel.

Measurement of retraction fibre tension using optical tweezers. Carboxylated polystyrene beads with a diameter of 0.958 μm (Polyscience) were trapped and calibrated using the power spectral density method[37]. The typical trap stiffness was 50 fN nm^{-1}. The bead was placed on a fibre for about 5 min. After the connection was tested, the bead was displaced 100 nm perpendicular to the length of the fibre, following a step protocol. This protocol gives the pulling force (F_p) and the total distortion (x) of the fibre. The tension (F_t) depends, in the first order, on the displacement x following the relation $F_t = F_p \times L/(4x)$. In the regime of small extension, the elasticity of the fibre does not contribute to the pulling force.

Cell stretching on flexible substrates. Fibronectin micropatterns were generated on thin silicon membranes (Gel pak PF-60-X4; thickness: 150 μm; Teltek). Membranes were clamped in a custom-made device allowing membrane stretching using a micrometric screw, with a maximal extension of ∼ 25% in ∼ 30 s. A rectangular polydimethylsiloxane chamber was attached onto the membrane using vacuum grease, and cells were cultivated for at least 4 h before stretching. Stretching was carried out in late prometaphase, as soon as a clear chromosome plate could be detected. Only cells that had been stretched more than 10 min before anaphase were considered for analysis.

For micropatterning, membranes were stretched to maximum extension and circular ring-shaped micropatterns were created through deep-ultraviolet illumination, using a small photomask. The membrane was then un-stretched, leading to oval ring-shaped micropatterns on which cells were seeded. Stretching to maximum extension during the experiment resulted again in circular ring-shaped micropatterns, excluding any effect of the adhesive pattern geometry and subsequent cell elongation on the observed spindle rotation[21,38,39]. Using ring-shaped micropatterns furthermore prevented cell adhesion below the cell body, so stretching was transmitted to the mitotic cell body only through retraction fibres.

Force estimation for stretching experiments. To estimate the change in the force field generated by retraction fibres on stretching, a simple mathematical model of the cell as a three-dimensional (3D) sphere connected by fibres to a 2D elliptical pattern was built using MATLAB software. Attachment points of the fibres to the cell body were placed around the cell equator, as observed in Fig. 1a. The cell was assumed to have 100 retraction fibres with a homogeneous density on the pattern, attached at the closest point on the cell body equator (as in ref. 13). The pattern was deformed to a circular ring and the fibre position calculated assuming no gliding of the fibre attachment point on the cell body, as shown in Fig. 3b. Each fibre was assigned a tension corresponding to the mean value measured in Fig. 2e, and the projected forces on the X and Y axes were calculated.

Live-cell imaging. Cell recordings were done using a Yokagawa CSU-X1 spinning head mounted on an Eclipse Ti inverted microscope (Nikon) for high-resolution imaging (×100 objective: Figs 1a, 4a and Supplementary Figs S3 and S4d; ×60 objective: Figs 4c, 5, 6, 8 and Supplementary Figs S5, S6; or ×20 objective: Fig. 3b), using an Eclipse TE 2000-E inverted microscope (Nikon) for recording chromosome plate movements (×10 objective: Supplementary Fig. S1) and using an Axio Observer inverted microscope (Zeiss) for recording chromosome plate behaviour after cells stretching (×20 objective; DNA stained with blue-fluorescing Hoechst 33342 stain, Fig. 3d). Microscopes were equipped with a Coolsnap HQ2 camera (Roper Scientific) and were controlled either by the Metamorph software (Universal Imaging) or by the Axio vision software (Zeiss).

To allow visualization of retraction fibres and subcortical actin structures that are less bright than the actin cortex itself, the gamma value was decreased uniformly for the following images: Figs 1b, 4a,c, 5a first row, 6a second row, Figs 7a,b, 8a,b, Supplementary Fig. S5, left column and Fig. S6.

Image treatment using ndsafir software. Images in Fig. 7a,b, in Supplementary Movies S7, S8 and images showing Lifeact staining in RPE1 cells (Supplementary Fig. S6) were denoised in 2D + time using ndsafir[40] (patch size = 3, iterations = 8 and Poisson–Gaussian variance stabilization). A weighted average between the original and the denoised images was obtained using 30% of the original and 70% of the denoised version.

Measure of subcortical actin structure residence time, intensity and penetration depth into the cytoplasm. HeLa cells expressing Lifeact–mCherry were recorded at a single confocal plane at a rate of one image every 15 s. Kymographs (70 pixel width) were generated along the main axis of the retraction fibres (bar and cross shape) or in the axis of the mitotic spindle (disc shape) and orthogonal to it (Fig. 5a). Each pair of resulting kymographs was scaled similarly, thresholded and boundaries of subcortical actin structures were detected manually. The actin cortex was not taken into account. Assigned regions were then measured for height (residence time), width (penetration depth into cytoplasm) and integrated intensity.

Measure of spindle movements. Cells expressing both Lifeact–mCherry and EB3–GFP were recorded at a single confocal plane at a rate of one image in each colour every 15 s. Cells with a mitotic spindle that was well formed and roughly aligned with the axis of the bar pattern were analysed.

A kymograph was made from a line (70 pixels in width) aligned with the bar pattern long axis (Fig. 8b,c). The values on the width of the line were averaged. From this kymograph, we extracted both the temporal signal of actin on each side of the cell using a line scan (Fig. 8d) and the position of each pole of the mitotic spindle after

DOI: 10.1038/ncb2269

image thresholding (Fig. 8e). A MATLAB routine calculated the slope of a robust linear fit of the spindle position (average of the position of both poles) in the time interval corresponding to each peak of the Lifeact–mCherry signal. Slopes above 10% were considered significant and were counted either as 'anti-correlated' when moving away from, or 'correlated' when moving towards, actin structures.

Statistics. Mean ± standard error was presented, except in Supplementary Fig. S2c, where mean ± s.d. was presented. To determine the significance between two groups, indicated in figures by two (P values ≤ 0.02) or three asterisks (P values ≤ 0.01), Student's t-test or the Chi-square test was used, as indicated in the figure legends. P values ≥ 0.05 were considered nonsignificant.

36. Azioune, A., Carpi, N., Tseng, Q., Thery, M. & Piel, M. Protein micropatterns: a direct printing protocol using deep UVs. *Methods Cell Biol.* **97,** 133–146 (2010).
37. Tolic-Norrelykke, S. F. & Schaffer, E. Calibration of optical tweezers with positional detection in the back focal plane. *Rev. Sci. Instrum.* **77,** 103101–103111 (2006).
38. Maniotis, A. J., Chen, C. S. & Ingber, D. E. Demonstration of mechanical connections between integrins, cytoskeletal filaments, and nucleoplasm that stabilize nuclear structure. *Proc. Natl Acad. Sci. USA* **94,** 849–854 (1997).
39. Hertwig, O. Ueber den Werth der ersten Furchungszellen für die Organbildung des Embryo. Experimentelle Studien am Frosch-und Tritonei. *Arch. Mikrosk. Anat.* **42,** 662–807 (1893).
40. Boulanger, J. *et al.* Patch-based nonlocal functional for denoising fluorescence microscopy image sequences. *IEEE Trans. Med. Imaging* **29,** 442–454 (2010).

nature cell biology

DOI: 10.1038/ncb2269

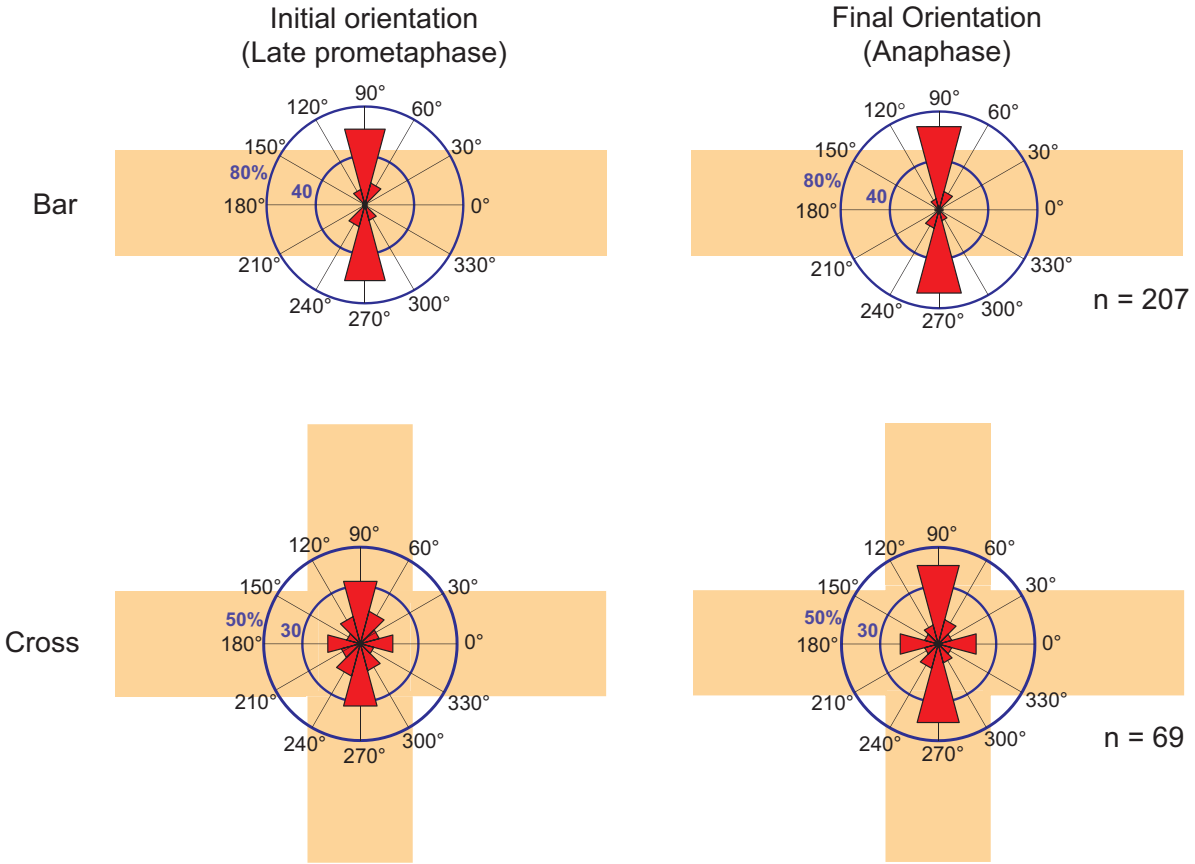

Figure S1 Chromosome plate orientations of HeLa cells dividing on bar and cross-shaped micro patterns. (**a**) HeLa cells expressing Histone-2B-mCherry to visualize chromosomes were recorded every 3 min during division. Circular graphs show the angular distribution of chromosome plate orientations (red) of cells dividing on bar or cross-shaped micro patterns (orange). Chromosome plate orientations in prometaphase (initial orientation) and one time point before anaphase (final orientation) are represented in angular sectors of 30º.

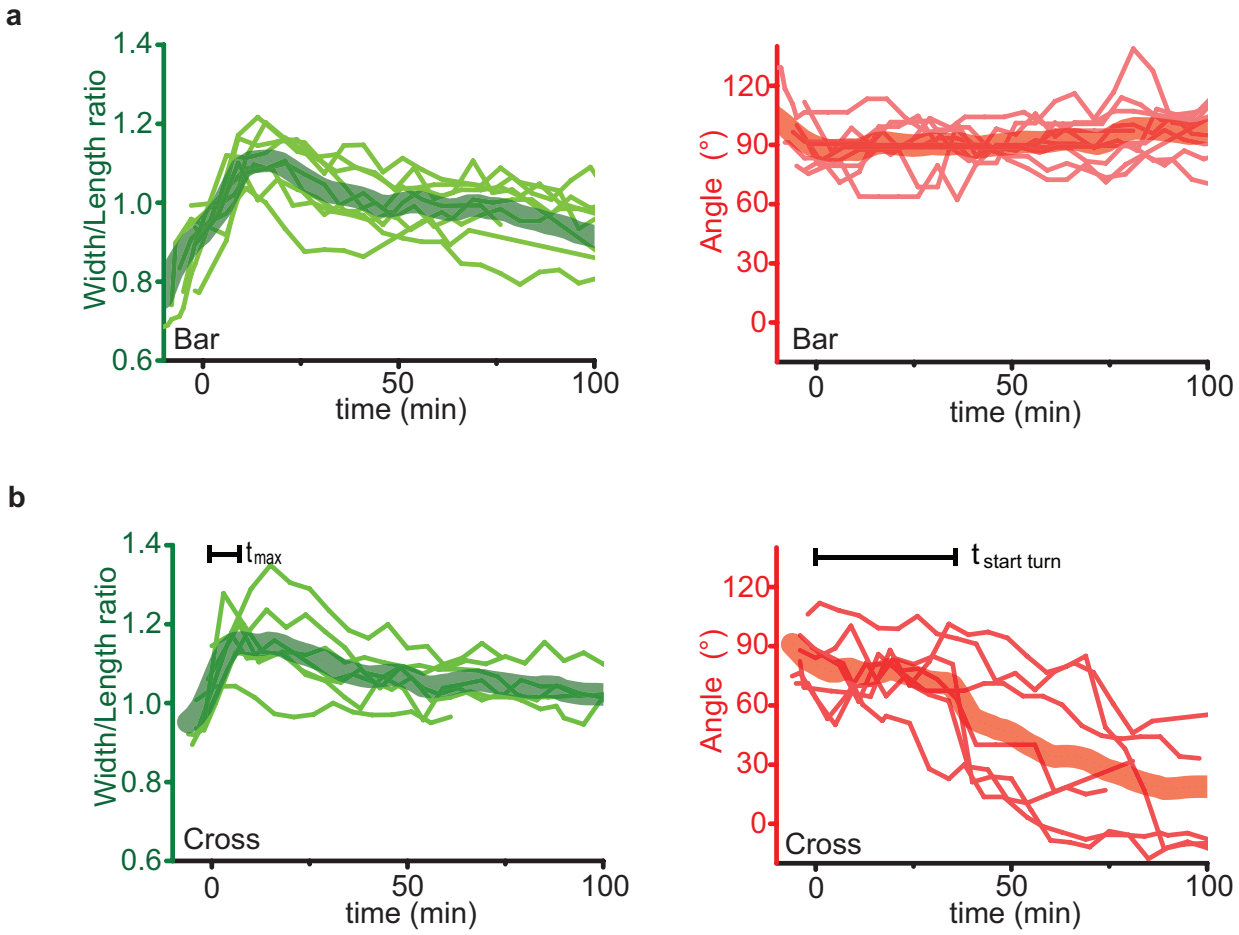

c

	W/L initial	W/L max	W/L start turn	t max	t start turn	
bar	0.89 +/- 0.06	1.13 +/- 0.06	-	15 +/- 5	-	n = 9
cross	0.99 +/- 0.08	1.21 +/- 0.10	1.08 +/- 0.07	9 +/- 5	32 +/- 22	n = 7

Figure S2 Cell body shape and chromosome plate angle after ablation of retraction fibres during mitosis. (**a+b**) Width/length ratio of the mitotic cell (left) and chromosome plate orientation (right) after retraction fibers ablation (at time 0 min), for single cells dividing on bar (**a**) and cross (**b**) shape. Thick lines represent average curves. (**c**) Table shows mean +/- standard deviation values of initial width/length ratio of the mitotic cell before laser ablation ($W/L_{initial}$), maximum width/length ratio after laser ablation (W/L_{max}), width/length ratio at beginning of spindle rotation (W/L_{turn}), time until maximum width/length ratio was reached (t_{max}), and time until spindle starts turning (t_{turn}).

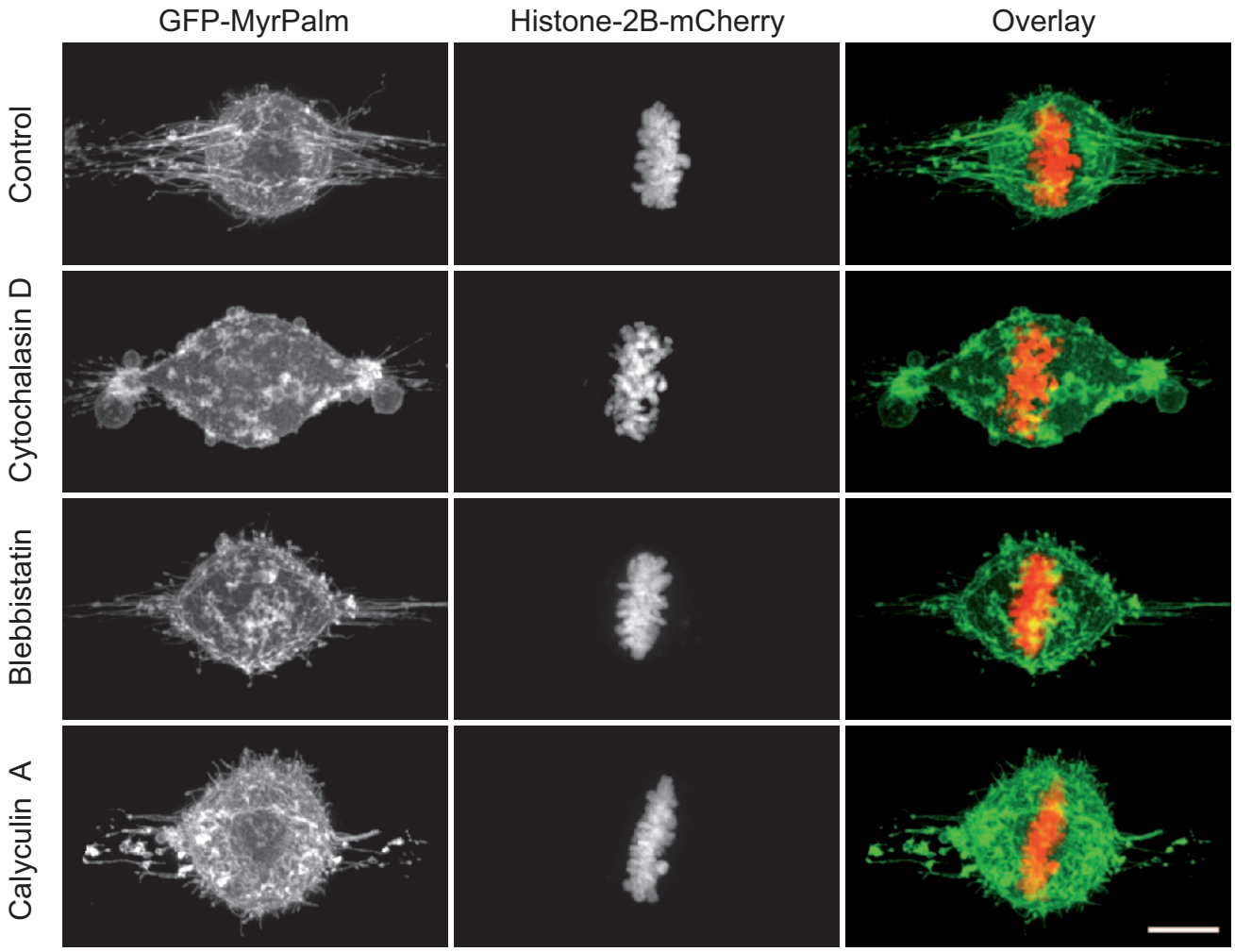

Figure S3 Actin and myosin 2 are required to maintain spherical cell body shape during metaphase. HeLa cells expressing MyrPalm-GFP and Histone-2B-mCherry to visualize membrane and chromosomes were allowed to round up during mitosis and were subsequently treated for 15 -30 min with different drugs acting on the acto-myosin system: control (first row), 1 µg/ml cytochalasin D (30 min, second row), 50 µM Blebbistatin (30 min, third row), 10 nM Calyculin A (15 min,fourth row). Scale bar, 10 µm.

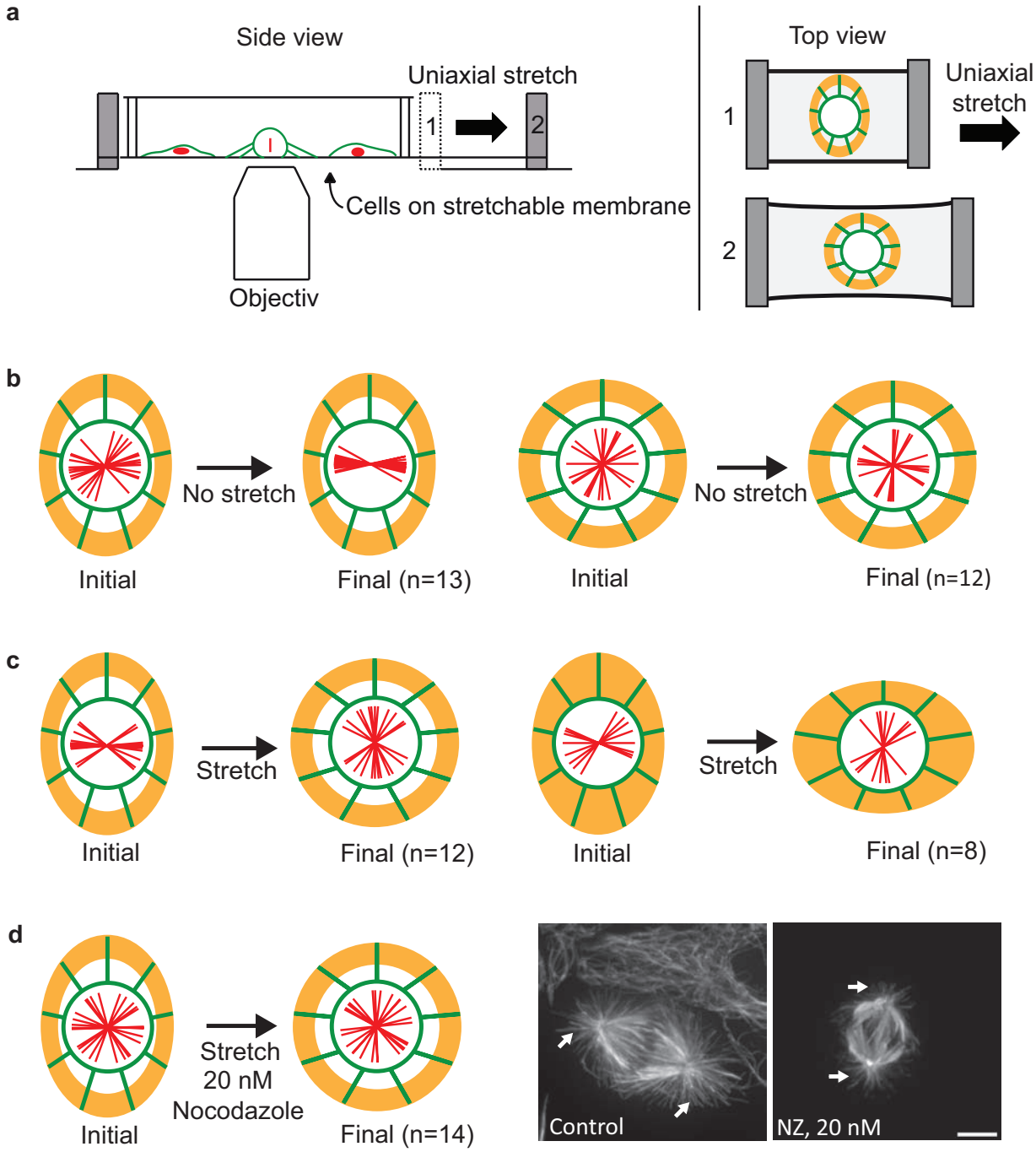

Figure S4 Stretching of retraction fibers induces spindle rotation dependent upon astral microtubules. (**a**) Schematic drawing of cell stretcher. (**b-d**) Chromosome plate orientation for RPE1 cells dividing on oval ring, ring or oval shaped micropatterns without (**b**) and with horizontal stretch (**c+d**). Chromosome plates were visualized by Hoechst 33342 staining of DNA and imaged every 3 minutes. 'Initial' represents chromosome plate orientation in late prometaphase – once chromosome plate can be clearly detected and at least 10 minutes before anaphase onset. 'Final' represents chromosome plate orientation at anaphase onset. Cells were stretched directly after imaging 'Initial' orientation. Graphics showing unstretched and stretched cells dividing on oval ring shaped micropatterns (left column, first and second row) are also shown in Fig 3. **(d)** Stretching of RPE1 cells dividing on oval ring shaped micropatterns in presence of 20 nM nocodazole (NZ). Low nocodazole concentration allowed depolymerization of astral microtubules without affecting spindle microtubules, as cells were not blocked in metaphase. Images show mitotic spindles (tubulin), actin cortex (phalloidin) and DNA (DAPI) in fixed control (left) and nocodazole treated cells (right). White arrows highlight astral microtubules. Micro-patterns, orange; chromosome plates, red; membrane, green. Scale bar, 10 μm.

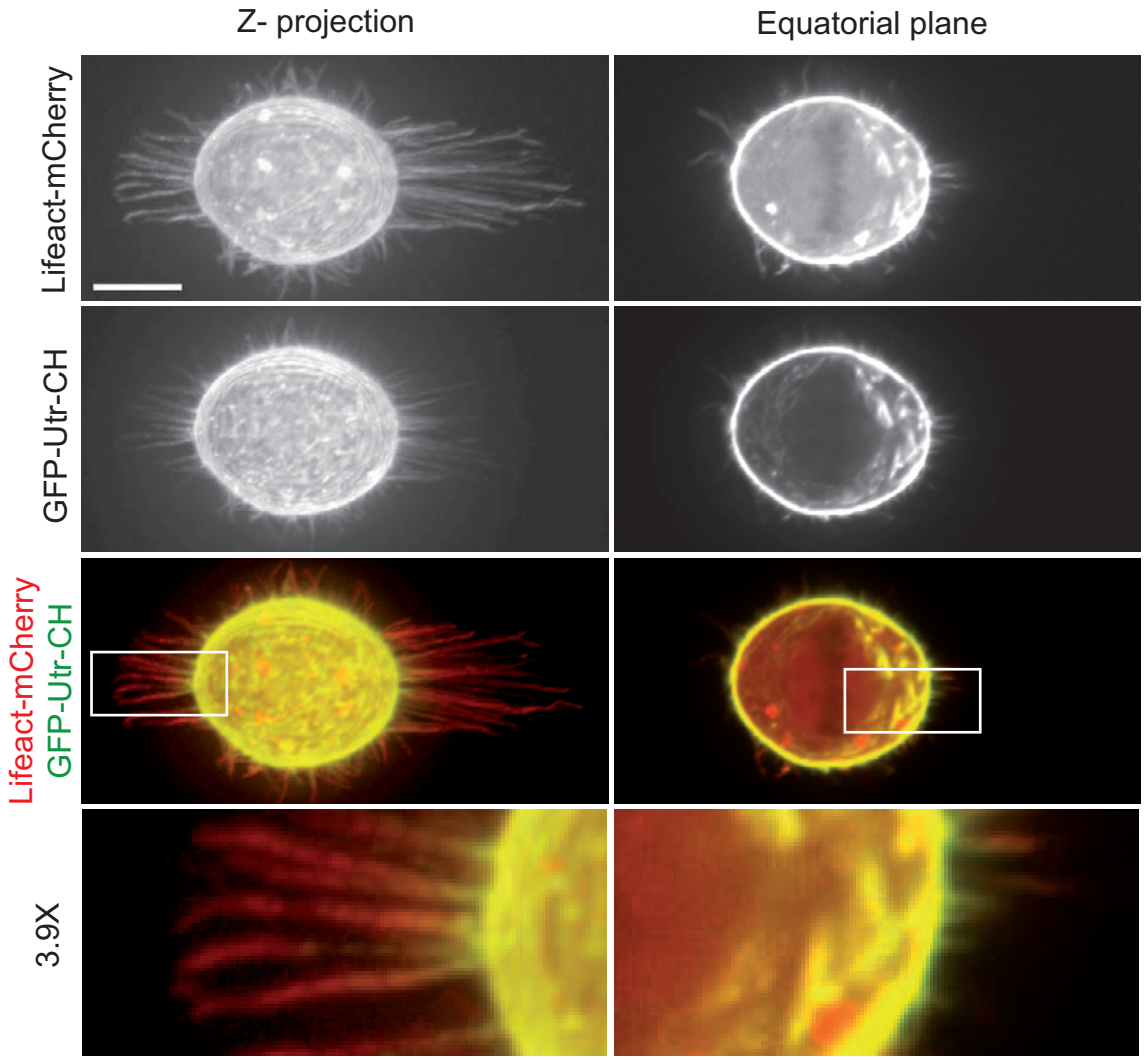

Figure S5 Comparison of Lifeact and Utr-CH –probes to visualize filamentous actin during mitosis. HeLa cell dividing on bar shaped micropattern and co-expressing Lifeact-mCherry and GFP-Utr-CH. Z-projections (left column) consist of images taken at 1 μm interval. Convincingly both actin probes visualize polarized actin structures found in the equatorial plane (right column). Note that rings appearing on the Z projection are due to the large spacing of the successive confocal planes. Actin filaments inside retraction fibers, which have been shown to be very stable[14], can be clearly visualized using Lifeact-mCherry. However GFP-Utr-CH appears to stain only actin filaments close to the cell body. Scale bar is 10 μm.

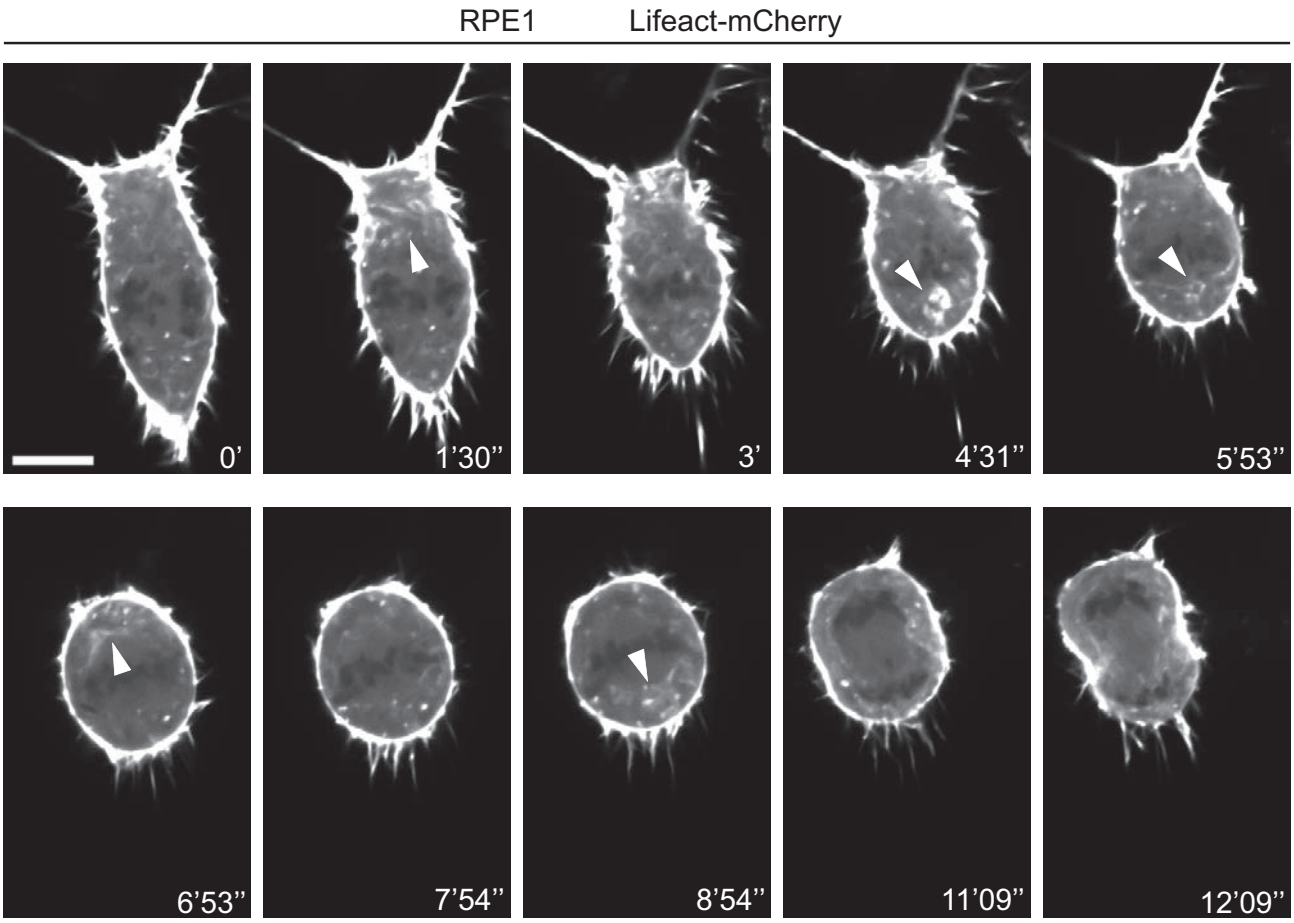

Figure S6 Subcortical actin structures in RPE1 cells. Timelapse sequence of a dividing RPE1 cell expressing Lifeact-mCherry. White arrows point out subcortical actin structures. Scale bar, 10μm. Time is in min (') sec (").

	Ratio (0/90 deg) of actin structures intensity		Penetration depth of actin structures into cytoplasm (µm) 0 deg	90 deg	ratio	Residence time of actin structures (min) 0 deg	90 deg	ratio	Rotation period (min)	Sense of rotation (%) CW	CCW	both	Cells with no or almost no actin at 90 degrees	
HeLa														
Bar (DMSO)	**1.9** *+/- 0.1*		**4.0** *+/-0.2*	**2.5** *+/- 0.2*	**1.7** *+/- 0.1*	**3.1** *+/- 0.1*	**2.9** *+/- 0.1*	**1.1** *+/- 0.1*	**6.1** *+/- 0.2*	25	45	30	6	n=20
Bar (20 nM NZ)	**2.4** *+/- 0.5*		**4.7** *+/- 0.6*	**2.6** *+/- 0.2*	**2.0** *+/- 0.4*	**3.4** *+/- 0.2*	**3.0** *+/- 0.2*	**1.2** *+/- 0.1*	**6.4** *+/- 0.4*	20	27	53	5	n=15
Cross	**1.5** *+/- 0.1*		**3.9** *+/- 0.3*	**2.9** *+/- 0.2*	**1.4** *+/- 0.1*	**2.9** *+/- 0.2*	**2.6** *+/- 0.1*	**1.1** *+/- 0.1*	**5.9** *+/- 0.3*	27	53	20	2	n=15
Disk	**1.1** *+/- 0.1*		**4.0** *+/- 0.2*	**3.7** *+/- 0.1*	**1.1** *+/- 0.1*	**2.7** *+/- 0.1*	**2.7** *+/- 0.1*	**1.0** *+/- 0.0*	**5.3** *+/- 0.1*	50	50	0	0	n=12
RPE1														
no pattern	-	-	**6.3** *+/- 0.6*	-	-	**2.7** *+/- 0.5*	-	-	**5.2** *+/- 0.4*	0	0	100	6	n=6

Table S1 Anisotropic distribution of retraction fibers induces a polarization of the sub-cortical actin structures in mitotic cells. Table showing quantification of subcortical actin structures behavior in HeLa cells dividing on different micropattern shapes and in RPE1 cells dividing on an uniform, non patterned substrate. Hela cells showing no or almost no actin at 90° were not taken into account for quantification of intensity, penetration depth and residence time of actin structures. Values represent mean +/- standard error.

Supplementary Movie Legends

Movie S1 Stretching of a dividing micro-patterned cell. Phase contrast time-lapse images of RPE1 cells plated on a micro-patterned silicon film. DNA was labeled with Hoechst and is shown in red. The timelapse is shown a second time with a zoom on the dividing cell. Time is shown on the upper left corner in minutes. Stretching is performed between times 3 and 6 minutes.

Movie S2 Dynamics of actin labeled by Lifeact-mCherry (in red) in HeLa cells plated on a circular pattern. EB3-GFP staining of the mitotic spindle is shown in green. Note the retraction fibers in the frames in which the focus is moved to the lower focal planes. Cytoplasmic actin structures are rotating around the cell periphery. Time is in min:sec

Movie S3 Dynamics of actin labeled by Lifeact-mCherry (in red) in HeLa cells plated on a bar pattern. EB3-GFP staining of the mitotic spindle is shown in green. Cytoplasmic actin structures are more intense and are penetrating deeper into the cytoplasm in the axis of retraction fibers (horizontal) than in the perpendicular axis. Time is in min:sec

Movie S4 Dynamics of actin labeled by Lifeact-mCherry (in red) in HeLa cells plated on an asymmetric cross pattern. EB3-GFP staining of the mitotic spindle is shown in green. Cytoplasmic actin structures are more intense and penetrate deeper into the cytoplasm in the main axis of the pattern (horizontal) than in the perpendicular axis. The mitotic spindle aligns with this polarization. Time is in min:sec

Movie S5 Dynamic s of actin labeled by Utr-CH-GFP (in green) in HeLa cells which were not plated on a patterned substrate. Chromosomes are visualized by H2B-mCherry (in red). Cytoplasmic actin structures are rotating around the cell periphery. Time is in min:sec

Movie S6 Dynamic s of actin labeled by Utr-CH-GFP (in green) in HeLa cells plated on a bar pattern. Chromosomes are visualized by H2B-mCherry (in red). Cytoplasmic actin structures are oscillating from one side of the cell to the other, facing retraction fibers. Time is in min:sec

Movie S7 Dynamics of actin structures (Lifeact-mCherry) before, during and after laser ablation of retraction fibres at 0 min in HeLa cells dividing on an asymmetric cross pattern. The mitotic spindle is visualized by EB3-GFP expression. After ablation of retraction fibres in the main axis of the cross pattern (horizontal), sub cortical actin structures polarize in the axis of remaining retraction fibres (vertical). The spindle follows this actin polarization and rotates to align with the axis of remaining retraction fibres/polarized actin structures. Time is in hour:min:sec

Movie S8 Dynamics of actin structures (Lifeact-mCherry) before, during and after laser ablation of retraction fibres at 0 min in HeLa cells dividing on a bar pattern. The mitotic spindle is visualized by EB3-GFP expression. After ablation of all retraction fibres, the polarization bias of subcortical actin structures in the main axis of the bar pattern (horizontal) is lost. The spindle does not rotate. Time is in hour:min:sec